Direct characterization of gas adsorption and phase transition of a metal organic framework using in-situ Raman spectroscopy

Kwanghee Jeong [a], Arash Arami-Niya [a,b], Xiaoxian Yang [a,c], Gongkui Xiao [a], Gregor Lipinski [c], Zachary M. Aman [a], Eric F. May [a], Markus Richter [a,c,*], Paul L. Stanwix [a,*]

[a] Fluid Science and Resources, School of Engineering, The University of Western Australia, Crawley, WA 6009, Australia
[b] Discipline of Chemical Engineering, Western Australian School of Mines: Minerals, Energy and Chemical Engineering, Curtin University, Perth, WA 6845, Australia
[c] Applied Thermodynamics, Chemnitz University of Technology, Reichenhainer Straße 70, 09126 Chemnitz, Germany

ARTICLE INFO

ABSTRACT

Adsorbents are widely used in gas separation and storage processes. Performance improvements are largely achieved through the continual development of new materials with unique sorption properties. Adsorption characterization techniques, therefore, play a central role in material research and development. Here, in-situ Raman spectroscopy is presented as a multi-purpose laboratory tool for analyzing adsorption performance. In contrast to conventional laboratory techniques requiring macroscopic samples, adsorption analysis via Raman spectroscopy can be performed on samples of less than 1 mg. Furthermore, simultaneous Raman multi-phase measurements of the adsorbent structure as well as the free and bound adsorbate, are shown to provide molecular insights into the operation of functional adsorbents at conditions representative of industrial applications, which are often not attainable in conventional crystallography. Firstly, a Raman-based method is demonstrated for directly quantifying absolute adsorption capacity within individual particles. The technique is validated for Raman measurements of carbon dioxide on silica gel and compared to gravimetric and volumetric analyses. Secondly, Raman spectroscopy is applied to study a novel functional material, ZIF-7, and directly probe its pressure-regulated gate-opening mechanism, which was only observed through indirect means. These Raman measurements confirm that the sharp increase in capacity corresponds to a structural transition in the material and reveal that multiple adsorption sites contribute to the overall capacity. The Raman methods presented here can be applied to a wide range of adsorbent-adsorbate systems and present a basis for further studies into the kinetics of sorption processes.

1. Introduction

Adsorbent materials are widely used in many industrial applications, ranging from energy production[1] through to water filtration[2] and environmental remediation[3]. For example, in the context of energy production, adsorbents play a critical role in natural gas processing[4], biogas production[5], and emission control for subsequent power generation[6]. In natural gas processing, they are employed for gas separations, including acid gas removal[7] and vent gas purification[8]. Advancements in materials and processes are continuously being pursued to improve performance and respond to contemporary challenges such as carbon capture,[9] helium separation,[10] and hydrogen storage.[11,12] In general, adsorbent materials are characterized by their capacity and selectivity for specified adsorbates, which can be

determined using well-established techniques, typically based on volumetric or gravimetric analyses, spanning different regimes of operation, including static[13] and dynamic[14] sorption, at low to high pressures, and from cryogenic to high temperatures.[15–18] A common feature of these methods is that the measurement itself is indirect and macroscopic, representing the average response over a suitable sample, imposing several measurement constraints including minimum sample sizes, insensitivity to material heterogeneity, and long acquisition times. With material development now focusing on understanding and designing adsorbents at the molecular level,[19] molecular simulation [20] as well as a range of advanced material characterization techniques including x-ray,[21] neutron,[22] and synchrotron[23] diffraction crystallography are being employed. However, these characterization tools are less suited to routine measurements, such as screening of

material candidates, and are typically limited to a narrow range of operation.

Raman spectroscopy provides an optical method for determining the composition of materials by probing the vibrational modes of the constituent molecules.[24] Raman spectrometers are increasingly being used as a laboratory-based characterization tool, due to their versatility, compact form, simplicity of operation, and reasonable cost. Monochromatic light (typically from a laser source) is scattered off a sample and detected using a spectrometer, with the resulting spectra exhibiting peaks at energy shifts related to the sample's molecular composition. [25] When performed through a microscope (i.e., Raman microscopy), the composition of a sample can be spatially resolved (imaged) with resolutions below 1 μm attainable, depending on the system's optical parameters.[26] At a basic level, the magnitude of each Raman peak is proportional to the density of corresponding molecules in the measured volume. Raman spectroscopy has been deployed in a wide range of fluid characterization applications, such as dew-point determination[27,28] and monitoring the composition of fuel components,[29–31] biogas, [32,33] air pollutants,[34,35] and hydrogen isomers.[36] For gas mixtures, relative concentrations can be determined by analyzing selected peaks associated with each component and their ratios.[37,38] The phase of molecules or their interaction with a nearby surface can also be identified from small changes in the Raman shift, intensity, and shape of each peak (provided the change can be resolved), for example, in clathrate hydrates[39] and water near hydrophobic surfaces.[40] In addition, this spectroscopic technique can monitor changes in solid structure, such as thermal deformation of graphene[41] and adsorbent cavity transformation.[42] Building off this wide-ranging sensitivity, the aim of this work is to demonstrate that Raman spectroscopy can provide direct and detailed observations of sorption processes, including direct quantification of adsorption capacity, through analysis of the adsorbate in optically compatible materials, as well as characterization of material performance and function, through analysis of the adsorbent, all acquired simultaneously and at process conditions.

Raman spectroscopy has previously been applied to various studies of adsorption. The authors recently reported a Raman-based method for measuring adsorption capacity in translucent materials, such as ionogels.[26] In contrast to the work presented here, that approach relied on an experimental correction factor, which can only be applied to systems where the signal from free gas molecules contained within the pores (henceforth referred to as free gas) and molecules adsorbed on the material surface (henceforth referred to as adsorbed gas) can be reliably deconvolved and compared to signal from the vapor phase outside the material (henceforth referred to as vapor-phase gas). Raman spectroscopy has also been applied to qualitative studies of sorption behavior. Panella and Hirscher[43] investigated the adsorbed phase of hydrogen on carbon nanotubes under ambient and cryogenic conditions. A range of studies looking at flexible metal–organic framework (MOF) adsorbents that employed Raman spectroscopy are summarized in Table 1. Of most relevance here is the work of Kontos and coworkers, who studied the adsorption of CO_2 on ZIF-69[44] (and later ZIF-68[45]) up to 1 MPa and from (273 to 337) K, showing qualitative agreement with gravimetric adsorption isotherms. Analysis of the adsorbent's Raman spectra identified one functional group that responded strongly with CO_2, with no structural modifications to the ZIF framework observed. Aside from this, Raman has generally been used as a qualitative tool in support of conventional characterization of MOFs. Also of note is the work of Kumari and coworkers, who reported temperature-induced structural changes in ZIF-8[46] and MOF-508[47]. The latter study used Raman with an anvil cell to look at pressure-induced structural changes in the adsorbate under very high pressure, albeit with a pressure transmitting medium and not the adsorbate. Aside from Raman spectroscopy, data from other characterization techniques, such as PXRD, IR, and TEM, have been employed to understand adsorbate function in support of conventional capacity measurements. However, whilst these techniques are widely used for understanding the functional structure of materials, they are not generally capable of directly observing adsorption-related phenomena at typical process conditions.

In this work, two methods for the characterization of adsorption based on high-resolution Raman spectroscopy are presented. These two methods are used to quantify adsorption capacity in optically transparent materials and probe the mechanism of adsorption in flexible adsorbents. For quantifying adsorption capacity, this work extends and generalizes previous work [26] by introducing a new method for measuring adsorption capacity using corrections based on the optical properties of the adsorbent material, which are independent of the Raman measurement (i.e., the optical signal corrections are not dependent on spectral deconvolution). The adsorption capacity for carbon dioxide within individual particles of silica gel is presented, and the results are validated against conventional bulk gravimetric and volumetric techniques. To study adsorption mechanisms in functional materials, Raman spectroscopy is used to simultaneously observe and correlate the response of both the adsorbent and adsorbate across pressure-regulated structural phase transitions. A qualitative comparison of in-situ Raman measurements with gravimetric measurements of the methane adsorption on ZIF-7 is presented, demonstrating that

Table 1

Summary of recent Raman spectroscopic studies on gas adsorption at a functional adsorbent.

	Adsorbent	Adsorbate	Raman measurement	Process variable	Comparative method
Nijem et al.[77] (2011)	Zn$_2$(bpdc)$_2$bpee	Nitrogen, Carbon dioxide	Adsorbent only	T = (83–293) K P = 0.1 MPa	N/A
Seo et al.[78] (2011)	Porous coordination polymer	Carbon dioxide	*Adsorbent, Gas*	T = 195 K P ≤ 0.1 MPa	Gravimetric
Kanoo et al.[79] (2012)	Fluoro-functionalized MOF	Carbon dioxide	*Adsorbent, Gas*	T = (173–323) K P ≤ 0.1 MPa	PXRD
Zhang et al.[80] (2012)	MAF-4	Nitrogen	Gas only	T = (83–297) K P = 0.1 MPa	PXRD
Nijem et al.[81] (2013)	FMOF-1	Methane	Gas only	T = (116–313) K P = 0.1 MPa	IR
Kumari et al.[46] (2013)	*ZIF-8*	Nitrogen Methane Carbon dioxide	*Adsorbent, Gas*	T[a] = (83–295) K P = 0.1 MPa	PXRD
Kontos et al.[44] (2014)	*ZIF-69*	Carbon dioxide	*Adsorbent, Gas*	T = (273–337) K P ≤ 1 MPa	Gravimetric
Kumari et al.[47] (2016)	MOF-508	Carbon dioxide	*Adsorbent, Gas*	T = 203 K, P = 0.1 MPa	N/A
Kontos et al.[45] (2020)	*ZIF-68* *ZIF-69*	Carbon dioxide	*Adsorbent, Gas*	T[b] = (198–353) K P[b] ≤ 1 MPa	Gravimetric; Molecular simulation
Kamali et al.[82] (2022)	*ZIF-7*	Carbon dioxide	*Adsorbent, Gas*	T = (263–301) K P ≤ 0.1 MPa	Volumetric
This work	*ZIF-7*	Methane	*Adsorbent, Gas*	T = 303 K P ≤ 4.1 MPa	Gravimetric

[a] Temperature range varies for each adsorbate.

[b] Temperature varied at P = 0.2 MPa, pressure varied at T = 311 K, different range for each adsorbent.

analysis of the Raman spectral features associated with the adsorbate can reveal correlations between pressure-induced structural changes in ZIF-7 with its adsorption capacity for methane.

2. Material and methods

2.1. Raman spectroscopic measurements

An overview of the Raman adsorption-characterization setup and measurement methods used in this work is presented in Fig. 1. Raman spectra were acquired using the inVia Raman microscope spectrometer (Renishaw), with 532 nm laser excitation source and spectral resolution of approximately 1 cm^{-1}. Each spectrum was acquired over 1 s integration at full laser power, corresponding to approximately 100 mW after the objective (Olympus SLMPLN 20x, NA 0.25). The diameter and depth of the focal region were measured to be 3 μm and 65.2 μm, respectively.[48] A custom high-pressure cell was used for in-situ measurement of gas adsorption, fabricated from 316 stainless steel with a sapphire window, described in detail elsewhere.[48] The cell pressure was controlled by a high-pressure syringe pump (260D, Teledyne) and monitored by a piezoresistive pressure transducer (PA-33x, Keller) with a manufacturer-specified uncertainty of 0.05% of full scale (70 MPa). The temperature of the cell was monitored by resistance temperature detectors (RTD PR-11, Omega) with an uncertainty in the measured temperature of 0.3 K, calibrated against a WIKA CTP5000 reference thermometer. The cell temperature was controlled by Peltier modules mounted on the four exterior sides of the cell. Pressure and temperature data acquisition and control were performed with custom programs implemented in LabView software. For spectroscopic measurements of gas adsorption, each spectrum was acquired one hour after the desired pressure and temperature conditions were reached, to obtain equilibrium adsorption capacity. (Further measurements after one hour did not show any deviating trend at the controlled thermodynamic condition)

### 2.2. Preparation of adsorbents

A commercially available silica gel (VWR UK, batch:13J180016) was used as a model adsorbent to demonstrate adsorption capacity measurements with Raman spectroscopy. The silica-gel granules were crushed, and smaller particles were selected for measurements, with a height of 200–300 μm and a width of 1–2 mm. The silica-gel particles were degassed under vacuum at 393 K for 12 h. After the initial degassing process, five silica-gel particles were placed within the high-pressure visual cell. To remove any impurities introduced during the short transfer time, the sample was kept under vacuum in the Raman cell at 343 K for a further 12 h. After this secondary degassing procedure, the system temperature was controlled to 303 K and high-purity carbon dioxide gas (purity 99.995%, BOC) was injected into the cell.

ZIF-7 sample (powder) was synthesized using procedures described elsewhere.[49–51] The sample was degassed at 433 K under vacuum for 24 h. The activated sample was lightly pressed into a sample holder within the high-pressure Raman cell, producing a smooth surface. Then, a secondary degassing (same procedure as the silica gel) was performed. Since the powder is optically opaque, Raman measurements were carried out by focusing on the surface of the sample. The system temperature was controlled at 303 K and a high-purity methane gas (purity 99.995%, Coregas Australia) was injected into the high-pressure cell. For each pressure condition, three repeat measurements were carried out, focusing on: (i) the vapor phase outside the adsorbent; and (ii) the top surface of the ZIF-7 sample.

3. Results and discussion

3.1. Quantifying adsorption capacity with Raman microscopy

To determine gas adsorption capacity in transparent adsorbent materials, such as the silica-gel presented here, a new method has been developed to directly probe the molecular density of the adsorbate, inside the adsorbent, using Raman microscopy. The method is based on a comparison of two Raman measurements of the adsorbate density: 1) measurements in the vapor phase that surrounds the adsorbent, to
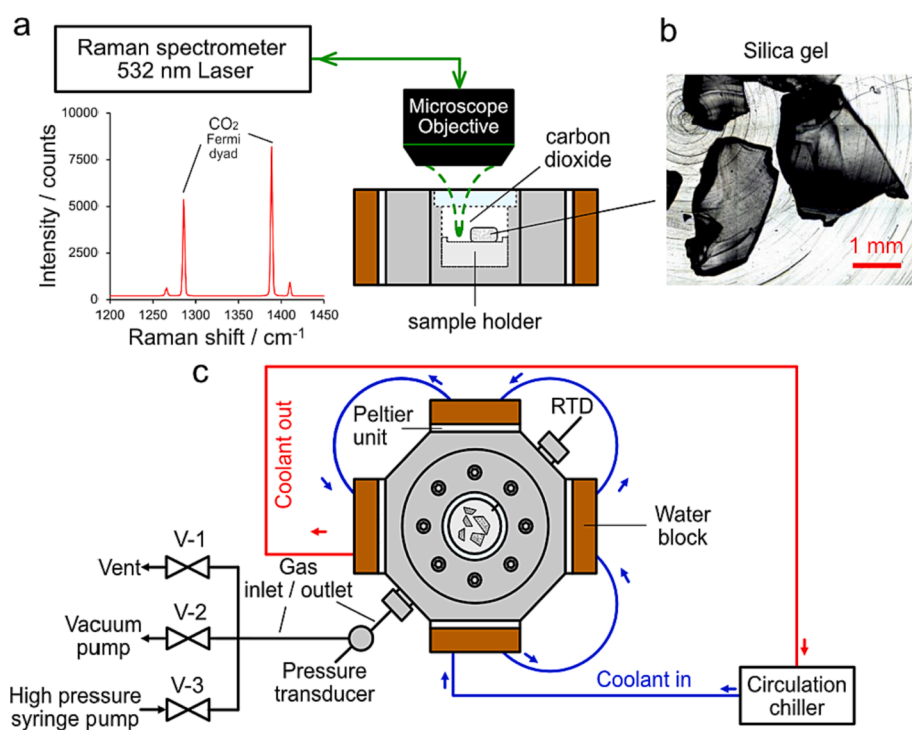
Fig. 1. An overview of the Raman system used for direct measurements of adsorption of CO_2 on silica gel or CH_4 on ZIF-7. (a) High-resolution Raman spectroscopy in conjunction with a microscope and high-pressure visual cell (side view) is used to measure the CO_2 density in the vapor phase (shown) and in the adsorbent material. (b) Optical image of the silica gel particles, showing their optical transparency. (c) Schematic overview of the experimental system, including the visual cell (top view).

determine the bulk-gas density; and 2) measurements within the adsorbent, to quantify the adsorbed and free gas densities. In contrast to conventional adsorption characterization techniques, which measure the average response over a macroscopic volume, Raman microscopy is a highly localized measurement of the average response over a microscopic volume. The inherent spatial resolution of Raman microscopy allows the measurement to reveal difference due to material inhomogeneity. To demonstrate the application of this technique and validate its quantitative capability, measurements of carbon dioxide adsorption on silica gel were performed using Raman microscopy and compared to conventional volumetric and gravimetric results.

3.1.1. Framework for analysis of Raman adsorption measurements

Measurements of adsorption are typically quantified in terms of net and excess adsorption. Net adsorption capacity can be defined as:

$$q_{net} = \frac{\rho_{a,molar} - \rho_{v,molar}}{\rho_{p,mass}} \tag{1}$$

where q_{net} is the net adsorption capacity, $\rho_{a,molar}$ and $\rho_{v,molar}$ are the molar densities of the adsorbate measured within the adsorbent and within the vapor phase, respectively, and $\rho_{p,mass}$ is the bulk mass density of the (porous material) adsorbent. In a general sense, q_{net} indicates the additional amount of adsorbate that can be contained within a system due to the presence of an adsorbent, compared to that of the container without the adsorbent.[52,53] For example, a gravimetric analyzer weighs adsorbent samples inside a container (i.e., the system). The buoyancy force for adsorbent samples in the presence of an adsorbate is compared to the weight of the sample under vacuum, with the difference being equivalent to the additional mass of adsorbate stored within the system volume at the measurement pressure and temperature.[54] Similarly, this work shows that Raman spectroscopy can be used to directly quantify net adsorption. The optical focal volume of the Raman apparatus (within which the Raman signal is excited and collected) is considered as the system. A microscope with an integrated translation stage allows the focal volume, which is smaller than a single particle of the adsorbent studied here, to be readily positioned inside or outside the adsorbent material, so that the Raman spectra can be acquired for the two states required to calculate net adsorption. (Note that ρ_v can be calculated from the measured Raman signal or from a suitable equation of state using the measured pressure and temperature for the system). The Raman spectral peak areas are converted to adsorbate densities by dividing the relevant Raman peak areas by the instrument-specific calibration factor (k_{cal}); it is posited that this value is also valid for measurements inside the adsorbent with the inclusion of optical corrections outlined below.

For measurements inside a transparent adsorbent material, the Raman signal must be corrected for the index of refraction. Corrections arise from the following mechanisms that are dependent on the change in refractive index between the vapor phase and the adsorbent material with adsorbed and free gas within its pores: i) changed apparent depth of the measurement volume;[55,56] ii) enhanced Raman-scattering cross-section;[57] and iii) reduced signal transmission at the particle interface as described by Fresnel equations. Therefore, the refractive index of the gas-filled porous medium is central to evaluating each correction. Whilst each of these phenomena have been reported separately over many decades across a range of fields, it is shown here for the first time the combined application of these concepts to Raman analysis of a porous system and quantifying adsorption capacity.

The effective refractive index of a heterogeneous system can be estimated using a model for the dielectric constant of a mixture and the properties of the constituent materials, for example, as proposed by Looyenga.[58] For an adsorbent material with gas-filled pores, as studied here, the refractive index is calculated using:[58,59]

$$n_{eff} = \left\{ (1 - \varnothing) n_{skel}^{2/3} + \varnothing n_{gas}^{2/3} \right\}^{3/2} \tag{2}$$

where n_{skel} is the refractive index of the adsorbent skeletal material (silica,[60,61] $n_{silica} = 1.46$) and n_{gas} is the refractive index of the free gas (carbon dioxide, calculated at the measured temperature and pressure using the model of Harvey and Lemmon,[62] implemented in REFPROP 10 [63]). The adsorbent porosity is given by:

$$\varnothing = 1 - \frac{\rho_p}{\rho_{skel}} \tag{3}$$

where ρ_p and ρ_{skel} are the bulk and skeletal densities of the adsorbent (porous) material.

The first correction, for the apparent depth of the focal volume, scales as the square of refractive index.[56] The second correction associated with the effect of refractive index on the Raman scattering cross section can be expressed through the local field factor, L, as discussed by Nestor and Lippincott[64]:

$$L = \left(\frac{n^2 + 2}{3} \right)^4 \tag{4}$$

The third correction for reduced signal transmission, which needs to account for two instances of transmission across the bulk gas-to-adsorbent interface, c_{trans}, can be calculated from Fresnel's equation assuming normal incidence by:

$$c_{trans} = \left\{ \frac{4 n_{eff} n_{co_2}}{\left(n_{eff} + n_{co_2} \right)^2} \right\}^2 \tag{5}$$

Considering all three correction terms outlined above, the corrected Raman peak area, $I_{Area,corr}$, can be written as:

$$I_{Area,corr} = I_{Area,meas} \bullet \frac{n_{gas}^2}{n_{eff}^2} \bullet \frac{L_{gas}}{L_{eff}} \bullet \frac{1}{c_{trans}} \tag{6}$$

where $I_{Area,meas}$ is the Raman peak area measured inside the porous medium. With the corrected area, eq (1) can be explicitly rewritten for Raman-based measurements as:

$$q_{net} = \frac{\left(\frac{I_{Area,corr}}{k_{cal}} \right) - \rho_{v,molar}}{\rho_{p,mass}} \tag{7}$$

The excess adsorption capacity (q_{ex}) includes the amount of adsorbate occupying the skeletal volume of a porous medium beyond the net adsorption capacity. This can be a useful term when quantifying adsorption because it is close to the absolute adsorption capacity under a low-pressure range. Accordingly, the excess adsorption capacity can also be expressed as:

$$q_{ex} = q_{net} + (1 - \varnothing) \frac{\rho_{v,molar}}{\rho_{b,mass}} \tag{8}$$

3.1.2. Spectra analysis and calibration of Raman density measurements

Raman spectra of free carbon dioxide molecules exhibit four peaks in the range (1200 to 1450) cm^{-1} (see Fig. 2). To quantify the density of carbon dioxide, the four peaks were simultaneously fitted with a Voigt profile and a linear background (Renishaw WiRE 3.4). The total area under the two major peaks (assigned to Fermi dyad)[65] was correlated with the molar density of carbon dioxide at the measured temperature and pressure, calculated using a reference equation of state for carbon dioxide (Span and Wagner,[66] implemented in the REFPROP 10 (NIST) [63]). At constant measurement conditions (temperature, optical path, laser power, exposure time), the Raman peak area was observed to increase linearly with gas molar density, providing a calibration for the conversion of spectral peak area to carbon dioxide molar density, as presented in Fig. 2. The gradient $k_{cal} = (1.37 \pm 0.01) \times 10^5$ (mol/L)$^{-1}$ represents an instrument- and condition-specific calibration constant needed to quantify carbon dioxide molar density at 303 K. This calibration was used in the adsorption capacity analysis, together with the three correction terms, to quantify the density of carbon dioxide
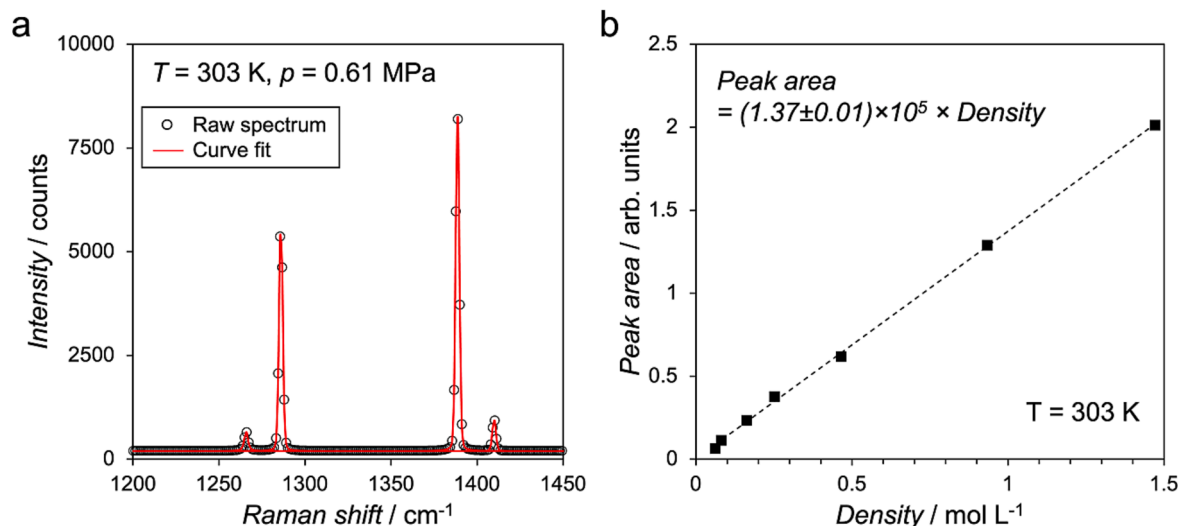
Fig. 2. (a) Raman spectrum of carbon dioxide gas (0.61 MPa). (b) Correlation between the total area of the two major carbon dioxide peaks and molar density at constant temperature and measurement conditions (see text).

molecules within the porous medium.

Raman measurements of the carbon dioxide within the silica gel were carried out by focusing inside the sample particle, halfway between the top and bottom particle surfaces (side view). As shown in Fig. 3, the Raman peaks associated with carbon dioxide were observed to both broaden and shift to lower wavenumbers. The redshift of the vibrational mode to lower wavenumbers can be attributed to adsorption, where the interaction of the gas molecules with the adsorbent material reduces the vibrational energy. This is consistent, for example, with the observations of Centrone et al.[67] using Raman spectroscopy, that Q-branch peaks of hydrogen molecules shifted to lower energy when adsorbed. For each pressure condition, to accurately estimate the adsorbent's characteristic adsorption behavior, measurements were performed at multiple locations and averaged, to account for possible material inhomogeneity. Five repeat measurements of the vapor phase were made at a single location, followed by measurements within the
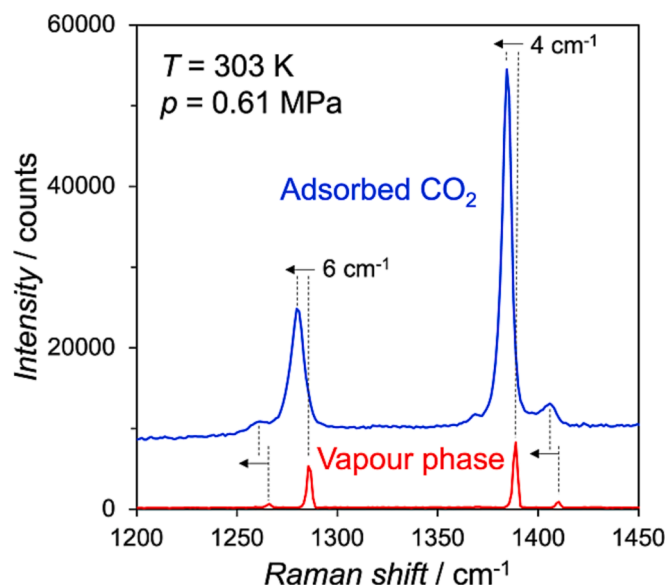
adsorbent particle at three locations, five repetitions at each. The results presented here are based on measurements of two particles, which were selected to have a top surface normal to the optical path. These two particles constitute a total measured sample mass of less than 1 mg.

3.1.3. Validation of Raman adsorption capacity technique

Silica gel's net adsorption capacity for carbon dioxide, measured using Raman microscopy, is presented in Fig. 4. Each data point represents the average of 30 measurements (two silica particles, three locations in each, five repetitions). The measurements are analyzed by first averaging the five repetitions for each location. The uncertainty of the Raman measurement is estimated from the standard deviation of the five repetitions, which is less than 1.0% for all locations and pressures. The results from the six locations are then averaged to arrive at a final Raman peak area for each pressure, with an associated standard error that is less than 5.2% for all pressures. Fig. 4 presents the Raman peak area for the measurement of carbon dioxide within the silica gel particles as a function of pressure. This signal was then converted to net-adsorption
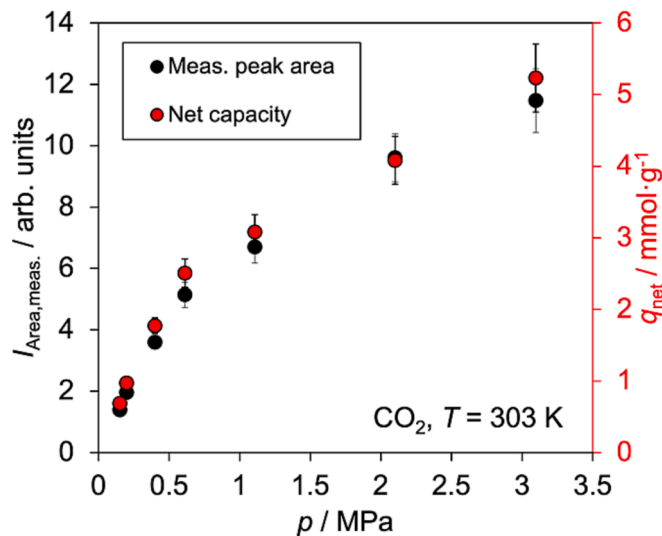

Fig. 3. Comparison of Raman spectra for carbon dioxide within a silica-gel particle (adsorbed CO_2) and in the vapor phase surrounding the particle. Adsorption results in a broadening and red-shift to lower wavenumbers of the Fermi-dyad peaks. Both spectra were measured at the same experimental conditions (the elevated background is due to the silica gel).

Fig. 4. Raman spectroscopic analysis on CO_2 adsorption to silica gel: (black) measured peak area profile of adsorbed CO_2 before corrections for refractive index, and (red) net adsorption capacity of silica gel converted from Raman peak area analysis, including corrections for refractive index.

capacity according to eq (7), and the results are presented in Fig. 4 (numerical results are tabulated in the Supporting Information). The error bars represent an estimate of the overall uncertainty in the adsorption capacity determined from Raman characterization. Uncertainty in the Raman adsorption capacity measurements arises from: the Raman signal, uncertainty described above; the conversion from Raman signal to molar density, for which the uncertainty was estimated as the standard error of the linear regression (see Fig. 2); the bulk density for the silica gel, uncertainty from material specification of 3%; and the calculation of the effective refractive index of the porous medium. The uncertainty in the effective refractive index (referring to eq (2)) is based on uncertainties for the refractive index of silica gel (less than 1%), refractive index of carbon dioxide (less than 1%), and porosity of the silica gel (3%). Here, an uncertainty of 5% is conservatively assumed for the effective refractive index of the silica gel in carbon dioxide. The conservative estimate of the uncertainty in the net-adsorption capacity measurement is 7.8%.

A silica gel sample from the same batch was measured using two conventional adsorption analysis techniques. A commercial gravimetric sorption analyzer (Rubotherm, TA Instruments) was used to measure the adsorption isotherm of carbon dioxide on silica gel at 303 K for pressures up to 4 MPa, with temperature and pressure uncertainties of 0.3 K and 0.01% full-scale (41 MPa), respectively. Detailed information about the measurement principle can be found elsewhere.[68] The isothermal gravimetric sorption capacity measurement was conducted twice to establish a level of reproducibility. Gravimetric sorption capacity measurements can provide direct measurements of a sample's net and excess adsorption capacities, with the latter coming from the former upon measurement of the adsorbent sample's buoyancy in the bulk fluid. Measurements of carbon dioxide adsorption on the silica gel were also carried out at 303 K and up to 0.12 MPa using a low-pressure volumetric sorption analyzer (ASAP 2020, Micromeritics), with details on the measurement procedure explained in detail elsewhere.[69] Volumetric techniques provide direct measurements of excess sorption capacity by using helium to determine the volume of the adsorbent sample. The excess adsorption capacities were measured with temperature and pressure uncertainties of 0.5 K and 0.15%, respectively. Numerical results for gravimetric and volumetric net and excess adsorption capacity measurements of silica gel for carbon dioxide are tabulated in the Supporting Information.

The excess adsorption capacity measured using all three techniques is presented in Fig. 5. At low pressures, the uncertainty of the pressure transducer used with the Raman cell becomes significant on a logarithmic scale; uncertainty bars are included to indicate the pressure transducer resolution. In practice, a suitable pressure transducer would be selected for the operating conditions of interest.

3.2. Raman analysis of pressure-regulated adsorption in flexible materials

The above results demonstrate Raman spectroscopy to quantify adsorption capacities, by directly observing the adsorbed molecules. However, a key attribute of the Raman method of sorption analysis is its ability to go beyond the information accessible through conventional measurements, which indirectly quantify adsorption. The Raman spectra can contain additional information about both the adsorbate and the adsorbent directly related to the underlying adsorption mechanism and process. For example, this can be demonstrated by considering adsorbents with regulated capacities, such as zeolitic imidazolate frameworks (ZIFs). ZIFs are a flexible metal–organic framework (MOF), comprising imidazole linkers and metal cations. These materials can undergo a structural phase transition in response to changes in pressure and temperature. In general terms, the lattice structure of the material transitions from a narrow pore (np) to a large pore (lp),[70] enabling a rapid and controllable increase in adsorption capacity. Therefore, these materials are being investigated for gas storage and separation applications.[71] For example, pressure-induced gate opening in ZIF-7 has
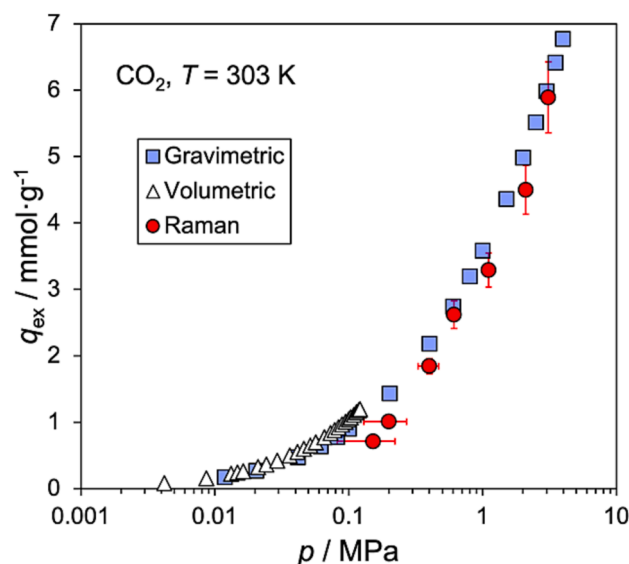

Fig. 5. Excess adsorption capacity of CO_2 on silica gel adsorbent, measured directly via Raman Spectroscopy and compared with the results from volumetric and gravimetric sorption analyzers. Uncertainty in adsorption capacity measurement (Raman) and associated pressure measurement are indicated by the vertical and horizontal error bars, respectively (note the logarithmic pressure scale).

been studied for the adsorption of methane, nitrogen and carbon dioxide using a gravimetric sorption analyser.[49,72,73] Since the gravimetric approach does not provide information on the structural state of the adsorbent, investigations of new materials rely on additional specialized characterization tools, which often cannot be operated across the same range of conditions; for example, ZIF-7 has been studied using X-ray diffraction.[74] Raman spectroscopy is a lower-cost and more widely available analytical technique; however, the application is not well established. This work demonstrates that Raman spectroscopy can provide direct insight into changing molecular structure in adsorbent materials, demonstrated on ZIF-7.

3.2.1. Review of Raman characterization of MOFs

A summary of gas adsorption in MOFs studies that include Raman spectroscopy is presented in Table 1. The studies vary in the extent to which Raman has been applied, ranging from qualitative assessment of isolated adsorbent material through to qualitative measurements of adsorbent and adsorbate across a range of temperature and pressure. In general, the results demonstrate observations of spectral variation of the adsorbent and an increasing trend of the adsorbate with gas uptake. However, in the presence of adsorbate, most of the spectral studies were conducted up to atmospheric pressure, with two studies up to 1 MPa. Diamond anvil cells have been used to achieve pressures in the giga-Pascal range (GPa), using a pressure transmitting medium (PTM) such as alcohol and silicon oil in place of the adsorbate to study a pressure-induced structural change of the adsorbent.[75,76] Raman measurements of pressure-induced structural change have not previously been reported.

3.2.2. Raman characterization of pressure-regulated structural transitions in ZIF-7

High-resolution Raman measurements of methane adsorption on a ZIF-7 material were performed at pressures up to 4.1 MPa, simultaneously observing the pressure-induced structural changes within the ZIF-7 framework and methane adsorption. Fig. 6a presents an example of the Raman spectra and deconvolution analysis of data acquired for methane adsorbed on a sample of ZIF-7 at 303 K at a pressure of 1.6 MPa. The region of the spectra corresponds to C-H stretching, with two peaks
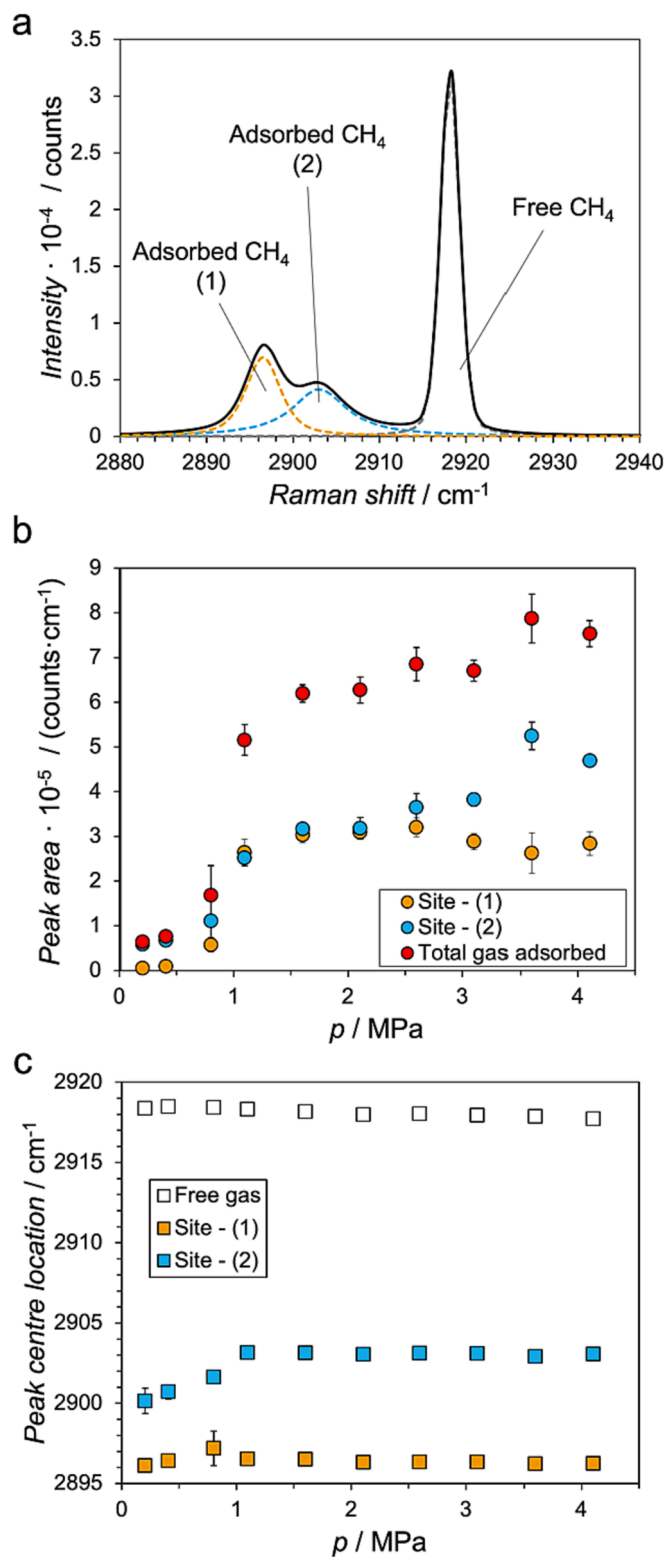
Fig. 6. Measurement of methane adsorption on ZIF-7 at varying pressure. (a) Example spectra illustrating the deconvolution of peaks associated with C-H bond stretching for free and adsorbed methane, measured at 303 K and 1.6 MPa. (b) Area of peaks defined in (a) attributed to two kinds of adsorption sites (1 and 2, identified with a peak center location). (c) Peak center location of the methane species for a free gas phase and adsorbed phase methane on sites 1 and 2.

associated with adsorbed methane and a free-methane peak. The first two peaks (which are not observed in the spectra of bulk vapor methane or the pure ZIF-7 adsorbent under vacuum, see supporting information Figure S1) exhibit different changes in peak area as the gas pressure is varied, as illustrated in Fig. 6. This observation leads us to propose that the two peaks correspond to two different classes of adsorption sites for methane on ZIF-7. This behavior with methane could be aligned with structural flexibility of ZIF-7 due to adsorbate migration between two types of six-membered ring pores, demonstrated by Zhao et al.[83].

Arami-Niya et al. [49] previously identified a pressure-induced structural transition of ZIF-7 by measuring the adsorption (physisorption) capacity of methane between 1 MPa and 1.5 MPa using the gravimetric technique. The measurement conditions were replicated here, with Raman spectra acquired as a function of pressure, as presented in Fig. 6. The responses of the two proposed adsorption sites are obtained by deconvolution of the combined peaks. The adsorption capacity of methane in the first class of ZIF-7 adsorption site (site (1) in Fig. 6) exhibits an evident change at the transition pressure, increasing from a capacity near zero to a relatively stable capacity at higher pressures. In contrast, the adsorption capacity of methane in the second class of ZIF-7 adsorption site (site (2) in Fig. 6) appears to exhibit an increasing adsorption capacity from low to high pressure in addition to the sharp increase at the transition pressure, indicating that site (2) is dominating in the large-pores. As shown in Fig. 6(c), a peak center location of the adsorbed gas molecules on site (1) was relatively stable over the pressure range, whereas the *gradual* blueshift up to the transition pressure was observed for the adsorbed molecules on site (2). This might indicate that the structural transformation was more closely linked to site (2), featuring larger energy of the adsorbed species than those on site (1).

The total adsorbed methane signal (sum of sites 1 and 2) is qualitatively compared to the capacity of methane on ZIF-7 reported by Arami-Niya et al.[49], presented in Fig. 7. The adsorbed-gas profile data obtained using Raman spectroscopy are in excellent qualitative agreement with the gravimetric measurement, with consistent critical pressure and relative change in the respective adsorption capacity signals.

Additionally, measurements with the Raman technique can provide insights into changes occurring in the adsorbent material. Fig. 8 presents Raman spectra measured for the ZIF-7 material over the wavenumber range 600–1400 cm^{-1}, revealing how several vibrational modes vary with pressure from vacuum to 4.1 MPa as methane adsorption occurs
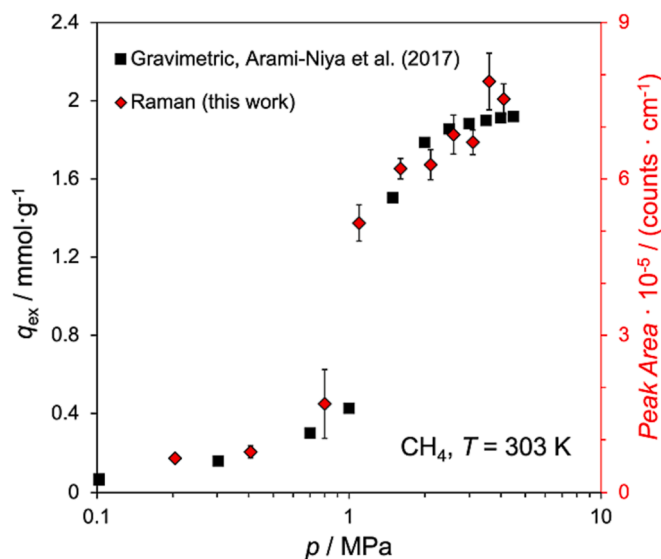
Fig. 7. A comparison of methane adsorption profiles measured by a gravimetric method[49] (adsorption capacity, black) and the Raman spectroscopic characterization (Raman peak area associated with adsorbed methane signals, red).
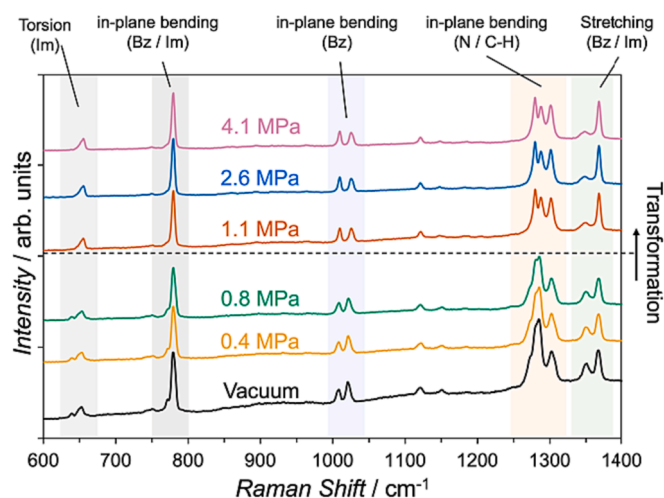
Fig. 8. Raman spectra of ZIF-7 at varying pressures of methane, indicating a structural transition occurred between (0.8 and 1.1) MPa. Each shaded band is assigned to a vibrational mode of a molecular bond; peak assignment in supporting information of ref.[85]. Each spectrum is offset vertically for clarity.

(select pressures are presented for clarity). The data and adsorption isotherm model for methane on ZIF-7 reported by Yang et al.[84] allow the transition pressure at 303 K to be calculated as $p_{tr} = (1.04 \pm 0.01)$ MPa. The peak shapes of the five torsional, bending, and stretching modes for the imidazole (Im) and benzene (Bz) groups in the ZIF-7 material all change qualitatively as the methane pressure passes through this transition pressure. This observation is consistent with a structural phase change occurring in the adsorbent ZIF-7 once a certain level of methane adsorption occurs.

Fig. 9 presents a more in-depth analysis of the torsion and in-plane bending modes of the benzene and imidazole ring, before and after the structural transformation. Furthermore, Fig. 10 shows the detailed analysis of a stretching mode of benzene and imidazole rings and an in-plane bending mode of (N / C-H) bond for imidazole rings. Deconvolution of the relevant peaks at each pressure was performed to investigate changes in peak parameters (peak center and full width half maximum (FWHM)). The most prominent change was an increase in the Raman shift of the peak location. The blueshift may be attributed to strain in the molecular system,[86] related to a compressed unit cell structure. This is consistent with the observation of Neimark et al.,[70] which reported adsorption-driven structural transition of MIL-53 adsorbents by mechanical pressure of carbon dioxide. Regarding the peak width, both narrowing and broadening were identified, which are associated with ordering and disordering,[87–89] respectively. Hence, the spectral analysis describes that shortened (possibly restricted) behavior of the vibrational modes and a locally changed ordering distribution are correlated with a particular enhancement of methane adsorption. Rahman et al.[90] identified the ZIF-7 structural phase transition is entropically-driven with the non-porous (low pressure) state being less ordered than large-pore (high-pressure) state. The insights provided here through Raman measurements of changes in the adsorbent's torsional and bending modes as the transition occurs could help clarify the nature of this entropically-driven transition and the mechanisms by which it is triggered.

4. Conclusions

This work demonstrates a novel application of a quantitative Raman analysis for in-situ gas adsorption studies and characterization of functional adsorbent materials. A commercial silica gel was used to adsorb carbon dioxide, and the adsorption capacity was directly quantified at a
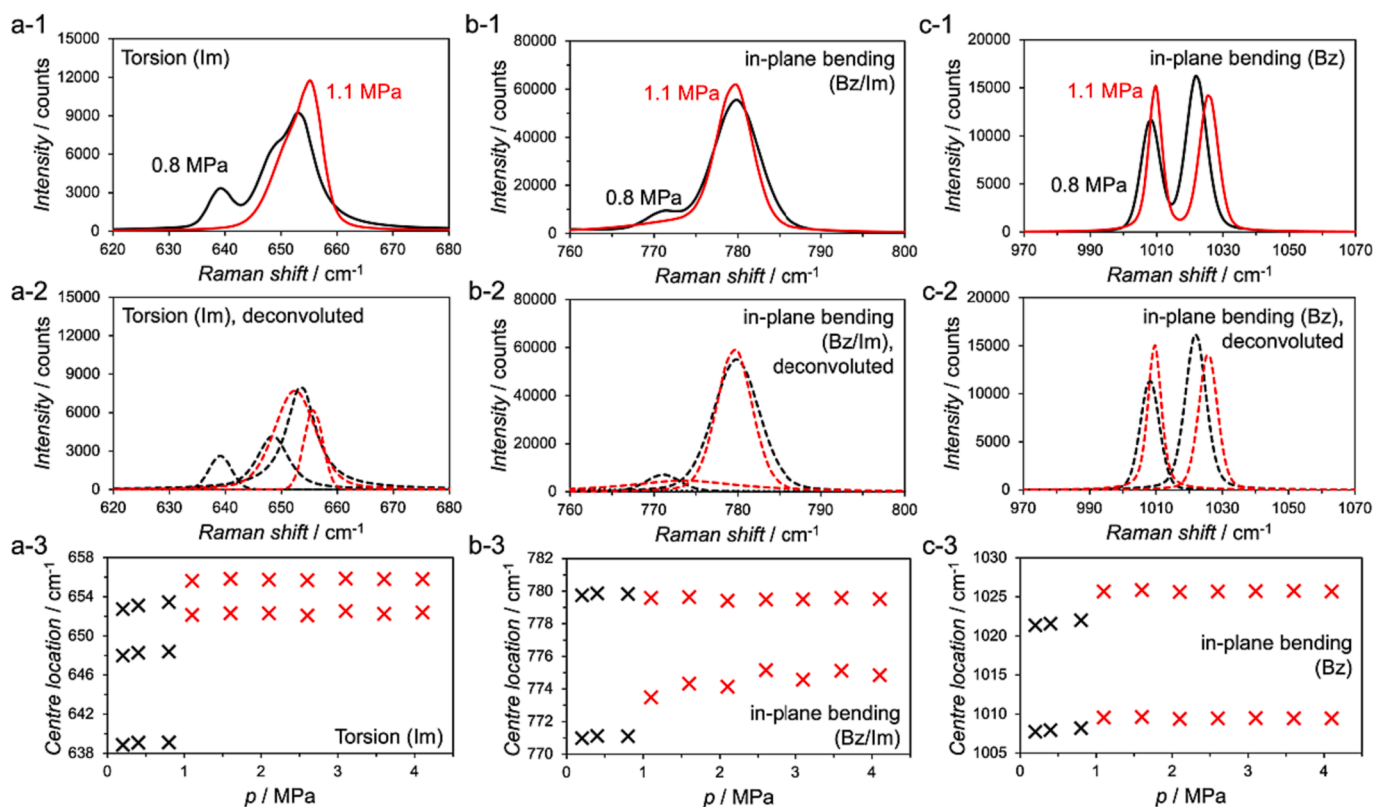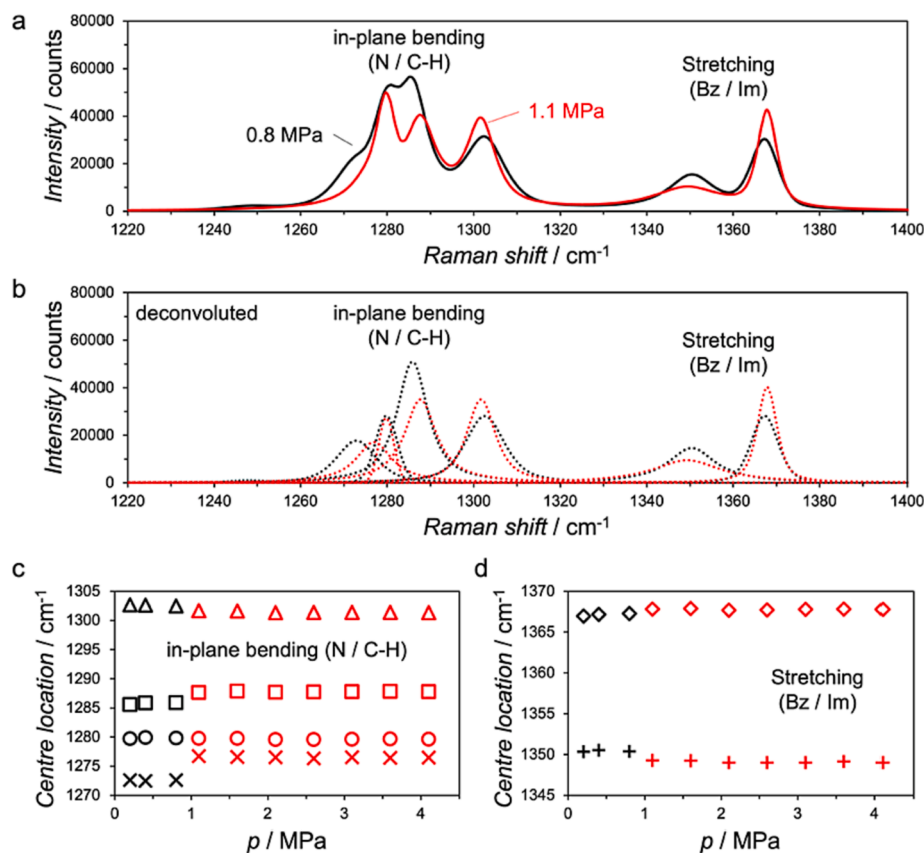

Fig. 9. Vibrational mode analysis of ZIF-7 in methane system across the gate opening (breathing) transition for panel a: torsion of imidazole ring (Im), panel b: in-plane bending through benzene and imidazole ring, and panel c: in-plane bending within benzene ring (Bz); each sub-panel presents for 1: acquired Raman spectrum, 2: deconvolution of the spectrum shown in (1), and 3: a peak center location of each deconvoluted peak.

Fig. 10. Vibrational mode analysis of ZIF-7 in methane across the gate opening (breathing) transition. (a) Acquired spectra of the in-plane bending mode of the (N/C-H) bond for imidazole rings and a stretching mode of the benzene and imidazole rings (Bz/Im). (b) Peak deconvolution of the spectra shown in (a) and peak center analysis (c-d) indicating the change in response across the transition pressure of 1.04 MPa.[84].

microscopic level using Raman spectroscopy, with a robust calibration method based on independently determined corrections necessary to accurately quantify the amount of adsorption occurring in a porous medium. It has also been shown that Raman spectroscopy can be used to probe the operation of functional absorbents at a microscopic level. Direct measurements of methane adsorption on ZIF-7 reveal correlations between the Raman spectral features for the adsorbate and adsorbent; significantly, the Raman technique allowed identification of two adsorption sites for the methane molecules on the ZIF-7 that varied in their uptake with pressure. Furthermore, qualitative changes in the torsional and bending modes of the imidazole- and benzene-ring groups in the adsorbent were apparent as the ZIF-7 underwent its structural phase transition at 1.04 MPa, with the blueshifts in these modes indicating that the increase in compressive strain is associated with the increased sorption capacity. In both studies, the data obtained were validated by comparison with conventional sorption analyzers, with excellent agreement over the measured pressure range for both carbon dioxide on silica gel and methane on ZIF-7. Overall, these results demonstrate that the Raman methods developed in this work provide a multifunctional approach for investigating and quantifying adsorption. Due to the flexibility and sensitivity of Raman spectroscopy, these methods can be applied to a wide range of adsorbent-adsorbate systems beyond the two systems presented in this work. Importantly, given the ability of Raman spectroscopy to uniquely resolve a range of molecular species, spatially and temporally, this technique has the potential to quantify adsorption selectivity and provide fundamental insights into the process of competitive adsorption. For functional adsorbents, a comprehensive study of the relationship between their Raman spectral features and material transitions will be necessary to understand the enhancement of adsorption capacity and thus design optimized functional materials.

CRediT authorship contribution statement

Kwanghee Jeong: Conceptualization, Methodology, Formal analysis, Investigation, Writing - original draft. **Arash Arami-Niya:** Investigation, Writing - review & editing. **Xiaoxian Yang:** Investigation, Writing - review & editing. **Gongkui Xiao:** Validation, Writing - review & editing. **Zachary M. Aman:** Funding acquisition. **Eric F. May:** Funding acquisition, Writing - review & editing. **Markus Richter:** Methodology, Funding acquisition, Supervision, Writing - review & editing. **Paul L. Stanwix:** Conceptualization, Methodology, Funding acquisition, Supervision, Writing - review & editing.

Declaration of Competing Interest

The authors declare that they have no known competing financial interests or personal relationships that could have appeared to influence the work reported in this paper.

Data availability

Data will be made available on request.

Appendix A. Supplementary data

Supplementary data to this article can be found online at https://doi.org/10.1016/j.cej.2023.145240.

References

[1] N. Hedin, L. Andersson, L. Bergström, J. Yan, Adsorbents for the post-combustion capture of CO2 using rapid temperature swing or vacuum swing adsorption, Appl. Energy 104 (2013) 418–433.

[2] D. Mohan, C.U. Pittman, Arsenic removal from water/wastewater using adsorbents—A critical review, J. Hazard. Mater. 142 (1) (2007) 1–53, https://doi.org/10.1016/j.jhazmat.2007.01.006.

[3] L. Mercier, T.J. Pinnavaia, Access in mesoporous materials: Advantages of a uniform pore structure in the design of a heavy metal ion adsorbent for environmental remediation, Adv. Mater. 9 (6) (1997) 500–503, https://doi.org/10.1002/adma.19970090611.

[4] M.A. Moreira, A.M. Ribeiro, A.F.P. Ferreira, A.E. Rodrigues, Cryogenic pressure temperature swing adsorption process for natural gas upgrade, Sep. Purif. Technol. 173 (2017) 339–356, https://doi.org/10.1016/j.seppur.2016.09.044.

[5] S. Cavenati, C.A. Grande, A.E. Rodrigues, Adsorption Equilibrium of Methane, Carbon Dioxide, and Nitrogen on Zeolite 13X at High Pressures, J. Chem. Eng. Data 49 (4) (2004) 1095–1101, https://doi.org/10.1021/je0498917.

[6] B. Feng, H. An, E. Tan, Screening of CO2 Adsorbing Materials for Zero Emission Power Generation Systems, Energy Fuel 21 (2) (2007) 426–434, https://doi.org/10.1021/ef0604036.

[7] H. Bamdad, K. Hawboldt, S. MacQuarrie, A review on common adsorbents for acid gases removal: Focus on biochar, Renew. Sustain. Energy Rev. 81 (2018) 1705–1720, https://doi.org/10.1016/j.rser.2017.05.261.

[8] T.L. Saleman, G. Li, T.E. Rufford, P.L. Stanwix, K.I. Chan, S.H. Huang, E.F. May, Capture of low grade methane from nitrogen gas using dual-reflux pressure swing adsorption, Chem. Eng. J. 281 (2015) 739–748, https://doi.org/10.1016/j.cej.2015.07.001.

[9] G. Xiao, R. Singh, A. Chaffee, P. Webley, Advanced adsorbents based on MgO and K2CO3 for capture of CO2 at elevated temperatures, Int. J. Greenhouse Gas Control 5 (4) (2011) 634–639, https://doi.org/10.1016/j.ijggc.2011.04.002.

[10] T.E. Rufford, K.I. Chan, S.H. Huang, E.F. May, A Review of Conventional and Emerging Process Technologies for the Recovery of Helium from Natural Gas, Adsorpt. Sci. Technol. 32 (1) (2014) 49–72, https://doi.org/10.1260/0263-6174.32.1.49.

[11] K.M. Thomas, Hydrogen adsorption and storage on porous materials, Catal. Today 120 (3) (2007) 389–398, https://doi.org/10.1016/j.cattod.2006.09.015.

[12] G. Li, J. Shang, Q. Gu, R.V. Awati, N. Jensen, A. Grant, X. Zhang, D.S. Sholl, J. Z. Liu, P.A. Webley, E.F. May, Temperature-regulated guest admission and release in microporous materials, Nat. Commun. 8 (1) (2017) 15777, https://doi.org/10.1038/ncomms15777.

[13] N.K. Jensen, T.E. Rufford, G. Watson, D.K. Zhang, K.I. Chan, E.F. May, Screening Zeolites for Gas Separation Applications Involving Methane, Nitrogen, and Carbon Dioxide, J. Chem. Eng. Data 57 (1) (2012) 106–113, https://doi.org/10.1021/je200817w.

[14] T. Saleman, G. Xiao, G. Li, E.F. May, A robust dynamic column breakthrough technique for high-pressure measurements of adsorption equilibria and kinetics, Adsorption 23 (5) (2017) 671–684, https://doi.org/10.1007/s10450-017-9884-3.

[15] J. Moellmer, E.B. Celer, R. Luebke, A.J. Cairns, R. Staudt, M. Eddaoudi, M. Thommes, Insights on Adsorption Characterization of Metal-Organic Frameworks: A Benchmark Study on the Novel soc-MOF, Microporous Mesoporous Mater. 129 (3) (2010) 345–353, https://doi.org/10.1016/j.micromeso.2009.06.014.

[16] G.C. Watson, N.K. Jensen, T.E. Rufford, K.I. Chan, E.F. May, Volumetric Adsorption Measurements of N2, CO2, CH4, and a CO2 + CH4 Mixture on a Natural Chabazite from (5 to 3000) kPa, J. Chem. Eng. Data 57 (1) (2012) 93–101, https://doi.org/10.1021/je200812y.

[17] T. Du, X. Fang, L. Liu, J. Shang, B. Zhang, Y. Wei, H. Gong, S. Rahman, E.F. May, P. A. Webley, G. Li, An optimal trapdoor zeolite for exclusive admission of CO2 at industrial carbon capture operating temperatures, Chem. Commun. 54 (25) (2018) 3134–3137, https://doi.org/10.1039/C8CC00634B.

[18] A. Arami-Niya, T.E. Rufford, G. Dresp, S. Al Ghafri, F. Jiao, E.F. May, Measurements of helium adsorption on natural clinoptilolite at temperatures from (123.15 to 423.15), Sep. Purif. Technol. 223 (2019) 1–9.

[19] C. Gu, N. Hosono, J.-J. Zheng, Y. Sato, S. Kusaka, S. Sakaki, S. Kitagawa, Design and control of gas diffusion process in a nanoporous soft crystal, Science 363 (6425) (2019) 387–391, https://doi.org/10.1126/science.aar6833.

[20] J. Zhang, J. Wang, C. Zhang, Z. Li, J. Zhu, B. Lu, Molecular simulation of gases competitive adsorption in lignite and analysis of original CO desorption, Sci. Rep. 11 (1) (2021) 11706, https://doi.org/10.1038/s41598-021-91047-0.

[21] K. Seki, Design of an adsorbent with an ideal pore structure for methane adsorption using metal complexes, Chem. Commun. 16 (2001) 1496–1497, https://doi.org/10.1039/B104204C.

[22] H. Wu, J.M. Simmons, G. Srinivas, W. Zhou, T. Yildirim, Adsorption Sites and Binding Nature of CO2 in Prototypical Metal−Organic Frameworks: A Combined Neutron Diffraction and First-Principles Study, J. Phys. Chem. Letters 1 (13) (2010) 1946–1951, https://doi.org/10.1021/jz100558r.

[23] Y. Kubota, M. Takata, T.C. Kobayashi, S. Kitagawa, Observation of gas molecules adsorbed in the nanochannels of porous coordination polymers by the in situ

[24] R.L. McCreery, Raman spectroscopy for chemical analysis, John Wiley & Sons, 2005.

[25] N. Colthup, Introduction to infrared and Raman spectroscopy, Elsevier, 2012.

[26] G. Lipinski, K. Jeong, K. Moritz, M. Petermann, E.F. May, P.L. Stanwix, M. Richter, Application of Raman Spectroscopy for Sorption Analysis of Functionalized Porous Materials, Adv. Sci. (2022) 2105477, https://doi.org/10.1002/advs.202105477.

[27] G. Lipinski, C. Holzammer, M. Petermann, M. Richter, Measurement of sorption phenomena near dew points of fluid mixtures: concept for the combination of gravimetric sorption analysis and Raman spectroscopy, Meas. Sci. Technol. 29 (10) (2018), 105501, https://doi.org/10.1088/1361-6501/aad49a.

[28] G. Lipinski, New Frontiers for Raman Spectroscopy: Investigation of Surface Phenomena and Gas Separation Processes, Applied Thermodynamics, Chemnitz University of Technology, 2021, p. 158.

[29] J. Kiefer, Recent Advances in the Characterization of Gaseous and Liquid Fuels by Vibrational Spectroscopy, Energies 8 (4) (2015) 3165–3197.

[30] J.C. Seitz, J.D. Pasteris, I.M. Chou, Raman spectroscopic characterization of gas mixtures. II. Quantitative composition and pressure determination of the CO2-CH4 system, Am. J. Sci. 296 (6) (1996) 577–600.

[31] A. Sieburg, A. Knebl, J.M. Jacob, T. Frosch, Characterization of fuel gases with fiber-enhanced Raman spectroscopy, Anal. Bioanal. Chem. 411 (28) (2019) 7399–7408, https://doi.org/10.1007/s00216-019-02145-x.

[32] S. Schlüter, T. Seeger, N. Popovska-Leipertz, A. Leipertz, Laserbasierte On-line-Analyse von Biogasen mit einer Raman-Sonde, tm -, Tech. Mess. 81 (11) (2014) 546–553, https://doi.org/10.1515/teme-2014-1050.

[33] T. Seeger, J. Kiefer, S. Eichmann, A. Leipertz, Raman spectroscopy based sensor system for fast analysis of natural and biogas composition, Advanced Photonics & Renewable Energy, Optica Publishing Group, Karlsruhe, 2010, p. p. STuB3..

[34] H. Inaba, T. Kobayasi, Laser-Raman Radar for Chemical Analysis of Polluted Air, Nature 224 (5215) (1969) 170–172, https://doi.org/10.1038/224170a0.

[35] S. Lederman, M.H. Bloom, Remote Measurement of Air Pollutants Utilizing the Raman Effect, in: E.S. Barrekette (Ed.), Pollution: Engineering and Scientific Solutions, Springer US, Boston, MA, 1973, pp. 438–452.

[36] L.-M. Sutherland, J.N. Knudson, M. Mocko, R.M. Renneke, Practical in-situ determination of ortho-para hydrogen ratios via fiber-optic based Raman spectroscopy, Nucl. Instrum. Methods Phys. Res., Sect. A 810 (2016) 182–185, https://doi.org/10.1016/j.nima.2015.12.009.

[37] A. Braeuer, In situ spectroscopic techniques at high pressure, Elsevier, 2015.

[38] P.L. Stanwix, N.M. Rathnayake, F.P.P. de Obanos, M.L. Johns, Z.M. Aman, E. F. May, Characterising thermally controlled CH4–CO2 hydrate exchange in unconsolidated sediments, Energ. Environ. Sci. 11 (7) (2018) 1828–1840, https://doi.org/10.1039/C8EE00139A.

[39] A.K. Sum, R.C. Burruss, E.D. Sloan, Measurement of Clathrate Hydrates via Raman Spectroscopy, J. Phys. Chem. B 101 (38) (1997) 7371–7377, https://doi.org/10.1021/jp970768e.

[40] H. Li, P. Stanwix, Z. Aman, M. Johns, E. May, L. Wang, Raman Spectroscopic Studies of Clathrate Hydrate Formation in the Presence of Hydrophobized Particles, Chem. A Eur. J. 120 (3) (2016) 417–424, https://doi.org/10.1021/acs.jpca.5b11247.

[41] D. Yoon, Y.-W. Son, H. Cheong, Negative Thermal Expansion Coefficient of Graphene Measured by Raman Spectroscopy, Nano Lett. 11 (8) (2011) 3227–3231, https://doi.org/10.1021/nl201488g.

[42] N. Nijem, H. Wu, P. Canepa, A. Marti, K.J. Balkus, T. Thonhauser, J. Li, Y.J. Chabal, Tuning the Gate Opening Pressure of Metal-Organic Frameworks (MOFs) for the Selective Separation of Hydrocarbons, J. Am. Chem. Soc. 134 (37) (2012) 15201–15204, https://doi.org/10.1021/ja305754f.

[43] B. Panella, M. Hirscher, Raman studies of hydrogen adsorbed on nanostructured porous materials, PCCP 10 (20) (2008) 2910.

[44] A.G. Kontos, V. Likodimos, C.M. Veziri, E. Kouvelos, N. Moustakas, G. N. Karanikolos, G.E. Romanos, P. Falaras, CO2 Captured in Zeolitic Imidazolate Frameworks: Raman Spectroscopic Analysis of Uptake and Host-Guest Interactions, ChemSusChem 7 (6) (2014) 1696–1702, https://doi.org/10.1002/cssc.201301323.

[45] A.G. Kontos, G.E. Romanos, C.M. Veziri, A. Gotzias, M.K. Arfanis, E. Kouvelos, V. Likodimos, G.N. Karanikolos, P. Falaras, Correlating vibrational properties with temperature and pressure dependent CO2 adsorption in zeolitic imidazolate frameworks, Appl. Surf. Sci. 529 (2020), 147058, https://doi.org/10.1016/j.apsusc.2020.147058.

[46] G. Kumari, K. Jayaramulu, T.K. Maji, C. Narayana, Temperature Induced Structural Transformations and Gas Adsorption in the Zeolitic Imidazolate Framework ZIF-8: A Raman Study, Chem. A Eur. J. 117 (43) (2013) 11006–11012, https://doi.org/10.1021/jp407792a.

[47] G. Kumari, N.R. Patil, V.S. Bhadram, R. Haldar, S. Bonakala, T.K. Maji, C. Narayana, Understanding guest and pressure-induced porosity through structural transition in flexible interpenetrated MOF by Raman spectroscopy, J. Raman Spectrosc. 47 (2) (2016) 149–155, https://doi.org/10.1002/jrs.4766.

[48] K. Jeong, Advanced Techniques to Study Interfacial Phenomena and Hydrate Nucleation, University of Western Australia, 2020.

[49] A. Arami-Niya, G. Birkett, Z. Zhu, T.E. Rufford, Gate opening effect of zeolitic imidazolate framework ZIF-7 for adsorption of CH4 and CO2 from N2, J. Mater. Chem. A 5 (40) (2017) 21389–21399, https://doi.org/10.1039/C7TA03755D.

[50] X. Wu, M. Niknam Shahrak, B. Yuan, S. Deng, Synthesis and characterization of zeolitic imidazolate framework ZIF-7 for CO2 and CH4 separation, Microporous

Mesoporous Mater. 190 (2014) 189–196, https://doi.org/10.1016/j.
micromeso.2014.02.016.

[51] K.S. Park, Z. Ni, A.P. Côté, J.Y. Choi, R. Huang, F.J. Uribe-Romo, H.K. Chae,
M. O'Keeffe, O.M. Yaghi, Exceptional chemical and thermal stability of zeolitic
imidazolate frameworks, PNAS 103 (27) (2006) 10186–10191.

[52] R. Pini, Interpretation of net and excess adsorption isotherms in microporous
adsorbents, Microporous Mesoporous Mater. 187 (2014) 40–52, https://doi.org/
10.1016/j.micromeso.2013.12.005.

[53] S. Gumma, O. Talu, Net Adsorption: A Thermodynamic Framework for
Supercritical Gas Adsorption and Storage in Porous Solids, Langmuir 26 (22)
(2010) 17013–17023, https://doi.org/10.1021/la102186q.

[54] X. Yang, A. Arami-Niya, J. Lyu, X. Guo, Net, Excess, and Absolute Adsorption of
N2, CH4, and CO2 on Metal-Organic Frameworks of ZIF-8, MIL-101(Cr), and UiO-
66 at 282–361 K and up to 12 MPa, J. Chem. Eng. Data 66 (1) (2021) 404–414,
https://doi.org/10.1021/acs.jced.0c00738.

[55] L.A. Woodward, J.H.B. George, Light flux received by a spectrograph from a
spatially extended refracting source, Proc. Phys. Soc. London, Sect. B 64 (9) (1951)
780–782.

[56] L.A. Woodward, J.H.B. George, Refractive Index Correction in Relative Raman
Intensity Measurements, Nature 167 (4240) (1951) 193, https://doi.org/10.1038/
167193a0.

[57] G. Eckhardt, W.G. Wagner, On the calculation of absolute Raman scattering cross
sections from Raman scattering coefficients, J. Mol. Spectrosc. 19 (1) (1966)
407–411, https://doi.org/10.1016/0022-2852(66)90262-1.

[58] H. Looyenga, Dielectric constants of heterogeneous mixtures, Physica 31 (3) (1965)
401–406, https://doi.org/10.1016/0031-8914(65)90045-5.

[59] V.I. Fesenko, I.A. Sukhoivanov, S.N. Shulga, Photonic crystals and microresonators
based on the anisotropic mesoporous silicon, Telecommun. Radio Eng. 70 (4)
(2011) 367–376.

[60] I.H. Malitson, Interspecimen Comparison of the Refractive Index of Fused Silica,
J. Opt. Soc. Am. 55 (10) (1965) 1205–1209, https://doi.org/10.1364/
JOSA.55.001205.

[61] N. Kitamura, Y. Toguchi, S. Funo, H. Yamashita, M. Kinoshita, Refractive index of
densified silica glass, J. Non Cryst. Solids 159 (3) (1993) 241–245, https://doi.org/
10.1016/0022-3093(93)90229-Q.

[62] A.H. Harvey, E.W. Lemmon, Method for Estimating the Dielectric Constant of
Natural Gas Mixtures, Int. J. Thermophys. 26 (1) (2005) 31–46, https://doi.org/
10.1007/s10765-005-2351-5.

[63] E. Lemmon, I.H. Bell, M. Huber, M. McLinden, NIST Standard Reference Database
23: Reference Fluid Thermodynamic and Transport Properties-REFPROP, Version
10.0, National Institute of Standards and Technology. 2018, https://www.nist.
gov/srd/refprop, 2018.

[64] J.R. Nestor, E.R. Lippincott, The effect of the internal field on Raman scattering
cross sections, J. Raman Spectrosc. 1 (3) (1973) 305–318.

[65] C. Holzammer, A. Finckenstein, S. Will, A.S. Braeuer, How Sodium Chloride Salt
Inhibits the Formation of CO2 Gas Hydrates, J. Phys. Chem. B 120 (9) (2016)
2452–2459, https://doi.org/10.1021/acs.jpcb.5b12487.

[66] R. Span, W. Wagner, A New Equation of State for Carbon Dioxide Covering the
Fluid Region from the Triple-Point Temperature to 1100 K at Pressures up to 800
MPa, J. Phys. Chem. Ref. Data 25 (6) (1996) 1509–1596.

[67] A. Centrone, D.Y. Siberio-Pérez, A.R. Millward, O.M. Yaghi, A.J. Matzger, G. Zerbi,
Raman spectra of hydrogen and deuterium adsorbed on a metal–organic
framework, Chem. Phys. Lett. 411 (4) (2005) 516–519, https://doi.org/10.1016/j.
cplett.2005.06.069.

[68] R. Kleinrahm, X. Yang, M.O. McLinden, M. Richter, Analysis of the systematic
force-transmission error of the magnetic-suspension coupling in single-sinker
densimeters and commercial gravimetric sorption analyzers, Adsorption 25 (4)
(2019) 717–735, https://doi.org/10.1007/s10450-019-00071-z.

[69] C. Wedler, K. Lotz, A. Arami-Niya, G. Xiao, R. Span, M. Muhler, E.F. May,
M. Richter, Influence of Mineral Composition of Chars Derived by Hydrothermal
Carbonization on Sorption Behavior of CO2, CH4, and O2, ACS Omega 5 (19)
(2020) 10704–10714, https://doi.org/10.1021/acsomega.9b04370.

[70] A.V. Neimark, F.-X. Coudert, C. Triguero, A. Boutin, A.H. Fuchs, I. Beurroies,
R. Denoyel, Structural Transitions in MIL-53 (Cr): View from Outside and Inside,
Langmuir 27 (8) (2011) 4734–4741, https://doi.org/10.1021/la200094x.

[71] B. Chen, Z. Yang, Y. Zhu, Y. Xia, Zeolitic imidazolate framework materials: recent
progress in synthesis and applications, J. Mater. Chem. A 2 (40) (2014)
16811–16831, https://doi.org/10.1039/C4TA02984D.

[72] J. Cai, Y.-Q. Tao, N. von Solms, C.-G. Xu, Z.-Y. Chen, X.-S. Li, Experimental studies
on hydrogen hydrate with tetrahydrofuran by differential scanning calorimeter and
in-situ Raman, Appl. Energy 243 (2019) 1–9, https://doi.org/10.1016/j.
apenergy.2019.03.179.

[73] D.-L. Chen, N. Wang, F.-F. Wang, J. Xie, Y. Zhong, W. Zhu, J.K. Johnson,
R. Krishna, Utilizing the Gate-Opening Mechanism in ZIF-7 for Adsorption
Discrimination between N2O and CO2, J. Phys. Chem. C 118 (31) (2014)
17831–17837, https://doi.org/10.1021/jp5056733.

[74] Y. Du, B. Wooler, M. Nines, P. Kortunov, C.S. Paur, J. Zengel, S.C. Weston, P.
I. Ravikovitch, New High- and Low-Temperature Phase Changes of ZIF-7:
Elucidation and Prediction of the Thermodynamics of Transitions, J. Am. Chem.
Soc. 137 (42) (2015) 13603–13611, https://doi.org/10.1021/jacs.5b08362.

[75] D. Radhakrishnan, C. Narayana, Guest dependent Brillouin and Raman scattering
studies of zeolitic imidazolate framework-8 (ZIF-8) under external pressure,
J. Chem. Phys. 144 (13) (2016), 134704, https://doi.org/10.1063/1.4945013.

[76] S. Chen, X. Li, E. Dong, H. Lv, X. Yang, R. Liu, B. Liu, Intrinsic and Extrinsic
Responses of ZIF-8 under High Pressure: A Combined Raman and X-ray Diffraction
Investigation, J. Phys. Chem. C 123 (49) (2019) 29693–29707, https://doi.org/
10.1021/acs.jpcc.9b08460.

[77] N. Nijem, P. Thissen, Y. Yao, R.C. Longo, K. Roodenko, H. Wu, Y. Zhao, K. Cho,
J. Li, D.C. Langreth, Y.J. Chabal, Understanding the Preferential Adsorption of CO2
over N2 in a Flexible Metal-Organic Framework, J. Am. Chem. Soc. 133 (32)
(2011) 12849–12857, https://doi.org/10.1021/ja2051149.

[78] J. Seo, C. Bonneau, R. Matsuda, M. Takata, S. Kitagawa, Soft Secondary Building
Unit: Dynamic Bond Rearrangement on Multinuclear Core of Porous Coordination
Polymers in Gas Media, J. Am. Chem. Soc. 133 (23) (2011) 9005–9013, https://
doi.org/10.1021/ja201484s.

[79] P. Kanoo, S.K. Reddy, G. Kumari, R. Haldar, C. Narayana, S. Balasubramanian, T.
K. Maji, Unusual room temperature CO2 uptake in a fluoro-functionalized MOF:
insight from Raman spectroscopy and theoretical studies, Chem. Commun. 48 (68)
(2012) 8487–8489, https://doi.org/10.1039/C2CC34276F.

[80] J.-P. Zhang, A.-X. Zhu, X.-M. Chen, Single-crystal X-ray diffraction and Raman
spectroscopy studies of isobaric N2 adsorption in SOD-type metal–organic zeolites,
Chem. Commun. 48 (93) (2012) 11395–11397, https://doi.org/10.1039/
C2CC35544B.

[81] N. Nijem, P. Canepa, U. Kaipa, K. Tan, K. Roodenko, S. Tekarli, J. Halbert, I.W.
H. Oswald, R.K. Arvapally, C. Yang, T. Thonhauser, M.A. Omary, Y.J. Chabal,
Water Cluster Confinement and Methane Adsorption in the Hydrophobic Cavities
of a Fluorinated Metal-Organic Framework, J. Am. Chem. Soc. 135 (34) (2013)
12615–12626, https://doi.org/10.1021/ja400754p.

[82] K. Kamali, S. Prasad, M.K. Sahoo, J.N. Behera, U.V. Waghmare, C. Narayana,
Unusual CO2 Adsorption in ZIF-7: Insight from Raman Spectroscopy and
Computational Studies, Inorg. Chem. 61 (30) (2022) 11571–11580, https://doi.
org/10.1021/acs.inorgchem.2c00913.

[83] P. Zhao, H. Fang, S. Mukhopadhyay, A. Li, S. Rudić, I.J. McPherson, C.C. Tang,
D. Fairen-Jimenez, S.C.E. Tsang, S.A.T. Redfern, Structural dynamics of a
metal–organic framework induced by CO2 migration in its non-uniform porous
structure, Nat. Commun. 10 (1) (2019) 999, https://doi.org/10.1038/s41467-019-
08939-y.

[84] X. Yang, A. Arami-Niya, G. Xiao, E.F. May, Flexible Adsorbents at High Pressure:
Observations and Correlation of ZIF-7 Stepped Sorption Isotherms for Nitrogen,
Argon, and Other Gases, Langmuir 36 (49) (2020) 14967–14977, https://doi.org/
10.1021/acs.langmuir.0c02279.

[85] P. Zhao, G.I. Lamproni, G.O. Lloyd, M.T. Wharmby, S. Facq, A.K. Cheetham, S.A.
T. Redfern, Phase Transitions in Zeolitic Imidazolate Framework 7: The Importance
of Framework Flexibility and Guest-Induced Instability, Chem. Mater. 26 (5)
(2014) 1767–1769, https://doi.org/10.1021/cm500407f.

[86] D.A. Strubbe, E.C. Johlin, T.R. Kirkpatrick, T. Buonassisi, J.C. Grossman, Stress
effects on the Raman spectrum of an amorphous material: Theory and experiment
on a-Si:H, Phys. Rev. B 92 (24) (2015), 241202, https://doi.org/10.1103/
PhysRevB.92.241202.

[87] H. Cynn, S.K. Sharma, T.F. Cooney, M. Nicol, High-temperature Raman
investigation of order-disorder behavior in the MgAl2O4 spinel, Phys. Rev. B 45 (1)
(1992) 500–502, https://doi.org/10.1103/PhysRevB.45.500.

[88] H. Cynn, O.L. Anderson, M. Nicol, Effects of cation disordering in a natural
MgAl2O4 spinel observed by rectangular parallelepiped ultrasonic resonance and
Raman measurements, Pure Appl. Geophys. 141 (2) (1993) 415–444, https://doi.
org/10.1007/BF00998338.

[89] H.-P. Liermann, R.T. Downs, H. Yang, Site disorder revealed through Raman
spectra from oriented single crystals: A case study on karooite (MgTi2O5), Am.
Mineral. 91 (5–6) (2006) 790–793, https://doi.org/10.2138/am.2006.2027.

[90] S. Rahman, A. Arami-Niya, X. Yang, G. Xiao, G. Li, E.F. May, Temperature
dependence of adsorption hysteresis in flexible metal organic frameworks,
Commun. Chem. 3 (1) (2020) 186, https://doi.org/10.1038/s42004-020-00429-3.